Journal of
Manufacturing and Materials Processing

MDPI

Article

Performance Evaluation of Graphene Nanofluid to Mitigate the Wear of a Diamond Tool in Micro-Machining of Ti6Al4V Alloy

Hongfei Wang, Qingshun Bai *, Shandeng Chen, Yuhao Dou, Wanmin Guo and Tingting Wang

School of Mechatronics Engineering, Harbin Institute of Technology, Harbin 150001, China; 20b908110@stu.hit.edu.cn (H.W.); sdchen@hit.edu.cn (S.C.); 18b908013@stu.hit.edu.cn (Y.D.); wmguo@hit.edu.cn (W.G.); wangtingting@stu.hit.edu.cn (T.W.)
* Correspondence: qshbai@hit.edu.cn

Abstract: Diamond tools are extensively used in ultra-precision machining due to their exceptional performance. However, when machining challenging materials like Ti6Al4V, diamond tools experience significant wear due to poor machining properties and catalytic effects. Tool wear not only impacts machining quality but also escalates machining costs and energy consumption. Cutting fluids are commonly employed to mitigate interfacial reactions and suppress tool wear. However, traditional cutting fluids are difficult to penetrate the cutting area and have limited lubrication and cooling capabilities. Therefore, in this paper, a technique combining graphene nanofluid and minimum-quantity lubrication (MQL) is used to suppress diamond tool wear. Firstly, micro-milling experiments for Ti6Al4V alloy are conducted using diamond tools in the graphene nanofluid MQL and under a dry environment. The experimental results show that tool wear is effectively suppressed by graphene nanofluids. Subsequently, the cutting process in both environments (graphene nanofluid MQL, dry) is simulated. The suppression mechanism of graphene nanofluid MQL for diamond tool wear is evaluated from phase transition, atomic transfer process, and amorphous behavior of diamond structure. The simulation results show that the contact characteristics, cutting force, and cutting temperature are improved by graphene nanofluids. Tool wear is effectively reduced. In addition, the removal efficiency of workpiece materials has also been improved. This work provides a technical basis for exploring the application of graphene nanofluids in diamond tool damage suppression and micro-milling.

Keywords: diamond tool; graphene nanofluid; minimum-quantity lubrication; wear mechanism

Citation: Wang, H.; Bai, Q.; Chen, S.; Dou, Y.; Guo, W.; Wang, T. Performance Evaluation of Graphene Nanofluid to Mitigate the Wear of a Diamond Tool in Micro-Machining of Ti6Al4V Alloy. *J. Manuf. Mater. Process.* **2023**, *7*, 131. https://doi.org/10.3390/jmmp7040131

Academic Editors: Bruce L. Tai and ChaBum Lee

Received: 25 June 2023
Revised: 15 July 2023
Accepted: 18 July 2023
Published: 19 July 2023

1. Introduction

Ti6Al4V alloys, with exceptional specific strength, superior corrosion resistance, and high-temperature strength, have been extensively utilized in diverse industries, including aerospace and biomedical engineering [1,2]. As technological advancements persist, there is a growing need for titanium alloys that exhibit increased resistance to high temperatures and enhanced strength. Alloying elements are added to the substrate to enhance its mechanical properties. According to the difference in microstructure, titanium alloy can be divided into α titanium alloy, β titanium alloy, and α + β titanium alloy [3–6]. Ti6Al4V (TC4) is one of the most widely used α + β titanium alloys with excellent overall performance. With the rapid development in aerospace, defense technology, and microelectronics, Ti6Al4V alloy microparts with high precision and complex shapes are urgently needed. For example, engine blades [7], metal hydrogen storage materials [8], boosters, and compressors [9]. However, with the traditional machining technology and equipment, it is difficult to achieve high precision, even with the high-efficiency processing of micro and small parts. The development of micro-cutting technology has become an inevitable choice.

Micro-milling has become one of the most widely used processes for micro-scale manufacturing due to its ability to machine workpieces with high precision and complex

surfaces [10]. However, the traditional underlying theories and methods no longer apply to micro-milling. Especially when machining difficult-to-machine materials such as Ti6AI4V by micro-milling, the rapid tool wear makes the production cost higher and the machining surface quality poorer [5,11,12]. The diamond tool is preferred as the material of choice for micro-milling tools due to its excellent physical properties. It can achieve high precision and mirror surface machining of parts [13,14]. However, diamond tools are also subject to wear and tear, affecting machining accuracy and quality and increasing energy consumption [15–17]. More importantly, the tool wear is also accelerated by the catalytic behavior of the transition elements on the diamond [18–20]. Therefore, it is crucial to reveal the failure mechanism of diamond tools and propose suppression measures. Zhang et al. [21] performed ultrasonic vibration cutting experiments on titanium alloys. The effect of cutting parameters on tool wear was explored. The results show that the amplitude and frequency of tool vibration are the most important factors affecting tool wear, the feed is a secondary factor on tool wear, and the depth of cut has the least effect on the amount of wear. Zareena et al. [22] investigated the mechanisms of tool wear involved in the ultra-precision machining of titanium. Graphitization from the characteristics of the tool, chip, and workpiece was found to be the mechanism that triggers tool wear. Park et al. [23] explored the wear mechanism of diamond drilling carbon fiber-reinforced plastics stacked on titanium. The diamond tools showed less titanium adhesion but a significant amount of cutting-edge chipping. Abrasion of carbon fibers and hard inclusions in Ti and adhesion of titanium was found to be the main tool wear mechanisms.

In order to improve tool life, scholars have proposed several auxiliary machining methods to suppress tool wear. Combining MQL with other techniques is considered one of the most effective methods. Gonzalez et al. [24] proposed a new lubrication technique for CO_2 + minimum-quantity lubrication. They found that cryogenic technology makes the use of PCD tools feasible, avoiding problems derived from the reactivity of Ti6Al4V alloy with this type of cutting tool. In addition, the machining process of carbon steel [25], Inconel 718 [26], Haynes 263, and Inconel 718 superalloys [27] has also shown that this new technology has excellent results in reducing tool wear and is more environmentally friendly. As another type of lubrication, the combination technology of nanofluid + MQL is also widely used. Nanofluid applications are widely used to improve the wear resistance and machining performance of tools [28,29]. It includes mainly base fluid and nanoparticles. The nanoparticles are mainly multi-walled carbon nanotubes [30], molybdenum disulfide [31], and graphene nanoparticles [32]. Among them, graphene nanoparticles are considered the first choice of additives for nanofluids due to their excellent thermal conductivity, lubricating properties, and chemical inertness [33,34]. Rakesh et al. [35] investigated the machining performance of nickel-based high-temperature alloys under graphene nanofluid. The results showed that tool wear was effectively suppressed by graphene nanofluid. The machining performance was best at 0.5 wt% graphene nanofluid with minimum tool wear. Anandan et al. [36] performed turning experiments on M42 steel in a graphene nanofluid environment. Graphene nanofluid significantly reduced surface roughness by 91%, tool wear by 95%, and cutting temperature by 82%. Recent advances in nanofluids in milling, turning, and grinding processes are summarized by Kursus et al. [37]. The results show that nanofluids are superior to other cooling and lubrication techniques. It improves the surface finish and reduces the cutting temperature, cutting force, and tool wear during machining. However, more research is still needed to determine their applicability in real industry, especially for using nanofluids in milling processes.

However, graphene nanofluid has been shown to possess excellent lubrication and machining properties in the machining of various materials. Additionally, less research has been conducted on applying the micro-milling of Ti6Al4V alloy with diamond tools. Therefore, this study researched the micro-milling of Ti6Al4V alloy with diamond tools under graphene nanofluid lubrication. First, graphene nanofluid milling experiments were performed. The tool wear state was characterized by scanning electron microscopy. The inhibitory performance of the nanofluid on tool wear was clarified. Next, cutting simulations

under a nanofluid environment were constructed based on the working conditions. The lubrication mechanism and the suppression mechanism of the catalytic effect of graphene on the diamond were revealed from the atomic perspective.

2. Experimental and Simulation Methods

2.1. The Micro-Milling Process

Ti6Al4V micro-milling experiments were performed three times on a 5-axis KERN-EVO machining center, as shown in Figure 1. The processing environment was configured for MQL of graphene nanofluid at room temperature. In order to verify the suppression performance of graphene nanofluids on tool wear, dry micro-milling was also performed under the same working conditions. Although only dry and graphene nanofluid conditions were tested in the micro-milling experiments and not pure base fluid (deionized water), related studies have confirmed that the lubrication and cooling performance of pure base fluid is inferior to that of graphene nanofluid [38]. This is mainly because the graphene nanoparticles, added as modifiers in the nanofluid, play a dominant role in determining the properties of the nanofluid [39]. Therefore, pure base fluid experiments were not conducted. More importantly, the regulation mechanism between the tool–workpiece interface was aimed to be revealed by this study rather than to compare the performance between water and graphene nanofluid. Consequently, the suppression mechanism of graphene nanofluid on tool wear and interface regulation mechanism was concentrated on in this study. The machine tool exhibits linear travel distances of 300 mm, 280 mm, and 250 mm along the X, Y, and Z axes, respectively, with a resolution of 0.1 μm. The annealed Ti6Al4V workpiece is divided into square-shaped pieces measuring 50 mm × 60 mm to facilitate the clamping of the workpiece. The vertical single-edged tool made of artificial monocrystalline diamond is employed for machining. This is mainly due to the higher hardness and lower friction coefficient of diamonds compared to conventional tools such as carbide tools. More importantly, diamond tools can be sharpened to nano-level precision to achieve extreme-parts manufacturing. It can meet the need for higher productivity [24]. The tool has a diameter of 1 mm and a cutting-edge length of 3 mm. The whole experiment involves two main parts. Firstly, the preparation of stable graphene nanofluid and the construction of the supply system. The cutting fluid in this study is a water-based graphene nanofluid with a mass fraction of 0.2% prepared by a two-step method, and the full dispersion of graphene nanoparticles in ion-free water is achieved by mechanical stirring and ultrasonic vibration, as shown in Figure 1c. In order to reduce the potential health hazards of graphene nanoparticles during the preparation and use of nanofluids, personal protective measures such as respiratory protective devices, protective clothing, and gloves should be promptly taken. In addition, when disposing of used graphene nanofluid waste, laboratory safety regulations should be strictly followed for disposal and recycling.

The MQL device injected the prepared graphene nanofluid into the cutting area, as shown in Figure 1d. To ensure the stability of the graphene nanofluid, it is used immediately after preparation. The MQL system operates with an air pressure of 0.5 MPa and a nozzle injection rate of 2.5 mL/min. Double nozzles are used in this study. Finally, the diamond micro-milling process of Ti6Al4V was carried out under the environment of MQL of graphene nanofluid. The spindle speed and feed rate were 94.2 m/min and 0.025 m/min, respectively. The milling path was cyclic end milling with a 100 mm cycle. The milling depth was 50 μm. During machining, the worker should wear protective clothes according to the requirements. Moreover, to solve worker health, always ensure that the hatch of the machine tool is closed to avoid the splashing of liquid from the MQL equipment. After processing, the machine tool should be cleaned under good safety protection measures, and the waste liquid should be disposed of according to the relevant requirements. The sealed waste liquid should be handled centrally and professionally.

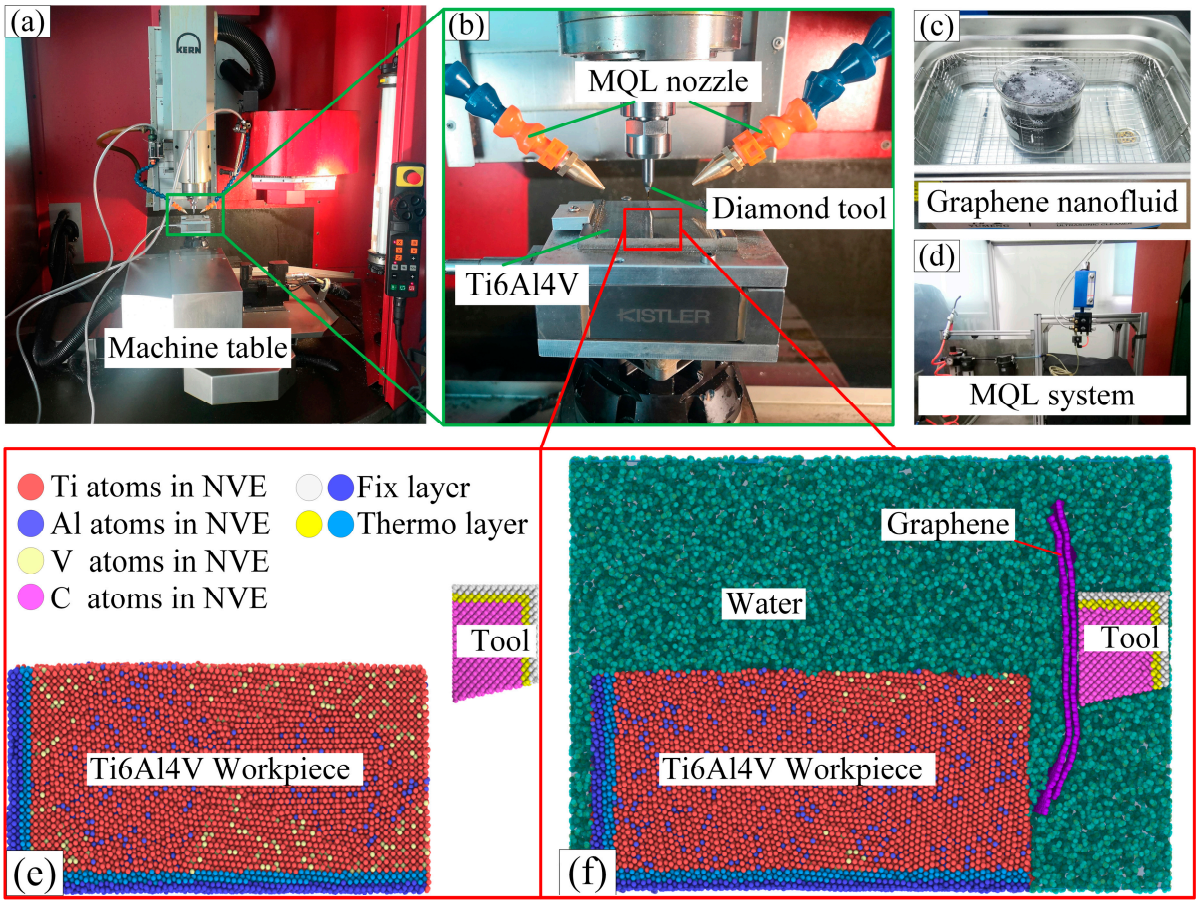

Figure 1. Experimental and simulation setup. (**a**) KERN-EVO machining center; (**b**) Machining platforms; (**c**) Graphene nanofluid; (**d**) MQL system; (**e**) Cutting simulation in a dry environment; (**f**) Cutting simulation in the graphene nanofluid.

2.2. MD Simulation Model

An atomic-scale analysis based on molecular dynamics was performed to investigate the suppression mechanism of graphene nanofluid on diamond tool wear. The molecular dynamics (MD) simulations are executed using the large-scale atomic parallel simulator (LAMMPS) [40]. Figure 1e shows the cutting model without graphene nanofluid, mainly consisting of a Ti6Al4V workpiece and diamond tool, i.e., dry cutting. The workpiece comprises 112,073 atoms with dimensions of 200 Å, 100 Å, and 100 Å along the X, Y, and Z directions, respectively. In order to keep the structure stable and prevent the workpiece from moving during the cutting process, the bottom and the left two atomic layers of the workpiece are set as boundary atoms. The two atomic layers near the boundary layer are thermostatic layers for the thermal equilibrium regulation of the system, and the model system is set to a Nose–Hoover. The remaining atoms obey the Newtonian layer of Newton's second law, which is used to respond to the mechanical properties of the material, i.e., the simulated system synthesis is an NVE ensemble [41–43].

The tool geometry is considered in the experiments when creating the tool model. The tool edge in the experiment is sharp rather than rounded. Therefore, the tool model is created for the simulation with a rake and rear angles of 0° and 9°, respectively. The tool is a diamond structure containing 9700 atoms and a lattice constant of 3.57. Consistent with the division of the atomic layers of the workpiece, it is also divided into the boundary, thermostatic, and Newtonian layers, respectively. The boundary layer is maintained to ensure structural stability and subjected to a velocity in the negative x direction to achieve the cutting process [44]. The actual machining situation was considered when creating the graphene nanofluid model. Part of the graphene particles are free at the tool edge during

machining, and the other part acts directly on the cutting edge. Among them, the graphene acting on the cutting edge is an important factor in suppressing tool wear. Therefore, the model is simplified to a graphene nanofluid cutting model acting directly on the cutting edge, as shown in Figure 1f. In contrast to dry cutting, the simulated environment is a nanofluidic environment composed of water molecules and graphene nanosheets, and the nanofluid filling is achieved by deposition. The detailed parameters of the model are shown in Table 1. The Nose–Hoover controlled the temperatures of water and graphene to simulate the heat exchange effect of the cutting fluid. For the reliability of the analysis, other settings are the same as for dry cutting. The simulations are first performed using the conjugate gradient method for energy minimization to optimize the model structure. Next, a relaxation process is performed under the NVT ensemble to ensure the model reaches equilibrium. Finally, the tool boundary layer atoms are given a constant speed of 20 mm/s along the negative x-axis direction to achieve the cutting process. The time step is 0.001 ps. In order to eliminate the effect of size on the simulation results, the x and y directions are set to periodic boundary conditions, and the z direction is set to fixed boundary conditions [45]. The open-source software Ovito does all visualization operations after the cutting simulation [46].

Table 1. System parameters of the cutting simulation.

Parameters	Value
Tool lattice structure	Diamond (single crystal diamond)
Workpiece lattice structure	HCP and BCC (Ti6Al4V alloy)
Total number of atoms in the workpiece	112,073
Total number of atoms in the tool	9700
Nanofluid type	Water-based graphene nanofluid
Cutting depth	15 Å
Cutting speed	2 Å/ps
Cutting length	200 Å
Equilibration temperature	300 K
Time step	0.001

Selecting an appropriate potential function to depict the atomic interactions in molecular dynamics simulations accurately is significant. Many researchers have done considerable research in the simulation of titanium alloys and diamond structures. The descriptions for titanium alloys are mainly the embedded-atom method potential (EAM) [47]. The structure of diamond and graphene is mainly described by LCBOP, Tersoff, and AIREBO potentials [48–50]. In this paper, the Ti, Al, and V interatomic interactions are depicted by the EAM potential [51]. The interactions between the C atoms of diamond and the C atoms of graphene and between diamond and graphene are described by the LCBOP potential. In addition, the Ti–C interactions are described by the comb3 potential function, and the morse potential characterizes Al-C and V-C. Van der Waals forces describe the potential of the remaining atoms and water molecules.

3. Results and Discussion

3.1. Suppression Performance of Graphene on Tool Wear

There are significant differences in structural form and dimensions between the single-edged micro-milling and traditional multi-edged tools. Criteria for evaluating the wear of micro-milling tools cannot be generalized. In this study, the contact area between the bottom face of the tool and the workpiece is the largest, and the most severe wear behavior is observed on the bottom surface. Therefore, the wear on the bottom face is only observed in subsequent analyses to determine the wear state of the tool. Figure 2 shows the wear morphology of the tool after machining 2000 mm under dry and graphene nanofluid conditions. The machining parameters are kept constant for both environments (spindle speed: 30,000 rpm, feed rate: 25 mm/min, depth: 50 μm). Although diamond

tools are extremely hard and wear-resistant, wear behavior is discovered when machining difficult materials such as Ti6Al4V, as shown in Figure 2b. In order to observe the tool wear morphology more clearly, the wear area is enlarged, as shown in Figure 2d,e. The wear morphology under the dry conditions shows that the workpiece material adheres to the bottom surface of the cutter tool, i.e., adhesive wear. It is mainly due to the adsorption of workpiece atoms by the tool atoms under the coupling effect of high shear stress and mechanical heat [52]. During the micro-milling process, the tool face undergoes friction and compression from the chips and workpiece, resulting in tool scratching. More importantly, the depth of scratches on the tool is exacerbated by the hard points of the workpiece, which ultimately leads to abrasive wear of the tool. In addition to the adhesive and abrasive wear, micro-chipping is observed in the cutting area. The observed phenomenon deviates from the progressive wear pattern typically observed in traditional tools. Instead, it exhibits a distinct cliff-like formation of cracks and chips. This distinctive behavior can be attributed to the inherent characteristics of diamond tools, which are characterized by their hardness, brittleness, and low coefficient of thermal expansion.

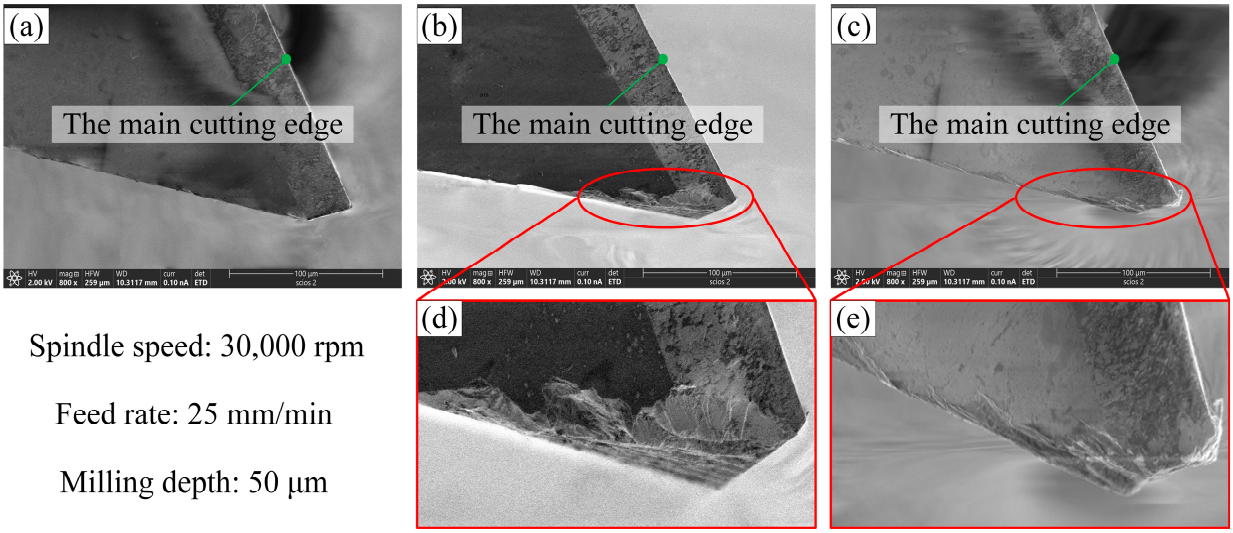

Figure 2. Diamond tool wear morphology in cutting Ti6Al4V alloy after 2000 mm machining distance. (**a**) A complete profile of the original tool; (**b**) wear profile under dry environment; (**c**) wear morphology under graphene nanofluid of MQL environment; (**d**) enlarged view of wear under environment; (**e**) enlarged view of wear under MQL environment.

The tool wear morphology under graphene nanofluid MQL is shown in Figure 2c,e. Compared to the dry state, there is an improvement in the size of the tool wear area and the form of wear. When graphene nanofluid is introduced during the machining process, the wear area on the bottom tool face is significantly reduced. Furthermore, the adhesive layer is found only at the tip. The results suggest that graphene nanofluid suppresses tool wear and improves the frictional characteristics of the tool–workpiece contact interface.

3.2. Dynamic Evolution of Tool Wear during Cutting Simulation

In order to examine the dynamic evolution process of tool wear suppression facilitated by graphene nanofluid, an analysis of the atomic-scale dynamic evolution process of tool wear was conducted using molecular dynamics, as shown in Figure 3. First, cutting simulation conditions were performed under graphene nanofluid. Next, cutting simulations were conducted under dry conditions to investigate the wear suppression effect of graphene nanofluid. The workpiece atoms and water molecules were removed to facilitate the observation of the tool atom wear process. The atomic structure of diamond tools is analyzed using the diamond structure identification method. The blue atoms represent the diamond structure, the purple atoms represent the graphene structure, and the gray atoms

represent the amorphous C atoms. Figure 3(b1–b5) represents the morphology of tool wear under dry cutting at different cutting distances. The results show that although the hardness of the diamond is much higher than that of Ti6Al4V, the diamond still undergoes structural transformation behavior, i.e., tool wear. Similar results have been found in cutting other materials [53,54]. As the machining distance increases, the tendency of diamond structure atoms to transform into amorphous carbon is intensified. It indicates that the service life of diamond tools is also limited. The diamond C-C bond is broken under impact loading and mechanical-thermo-chemical reactions.

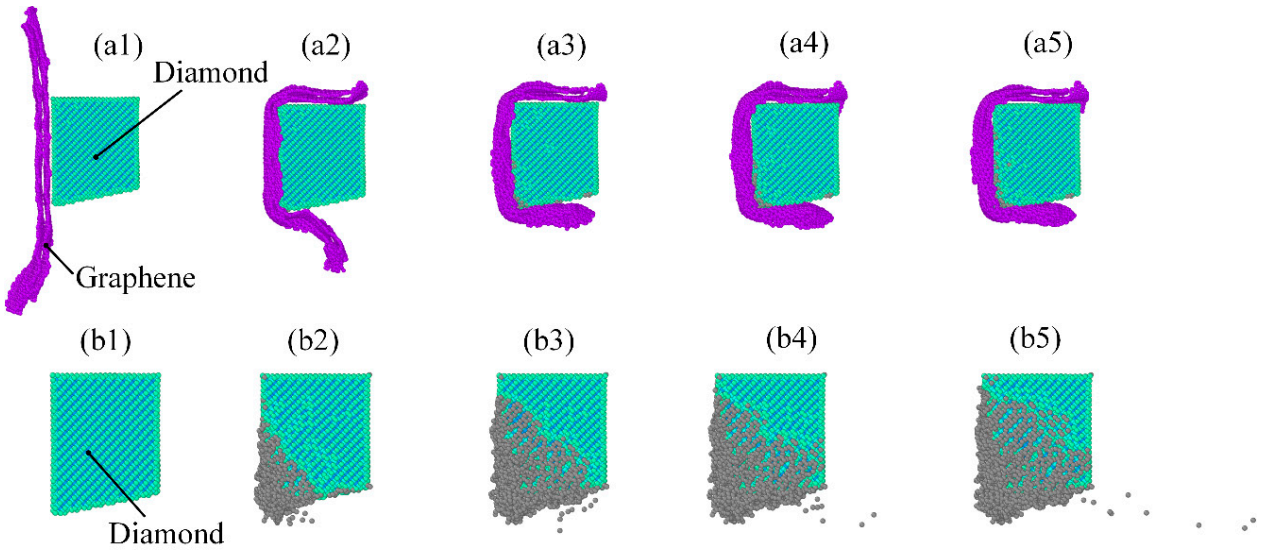

Figure 3. Dynamic evolution of tool wear. (**a1**) Initial state of the nanofluid model. (**a2**) Cutting distance of 44 Å. (**a3**) Cutting distance of 88 Å. (**a4**) Cutting distance of 132 Å. (**a5**) Cutting distance of 176 Å. (**b1**) Initial state of the dry model. (**b2**) Cutting distance of 44 Å. (**b3**) Cutting distance of 88 Å. (**b4**) Cutting distance of 132 Å. (**b5**) Cutting distance of 176 Å.

The tool wear is accelerated, especially by the mechanical-thermo-chemical reaction, mainly attributed to the catalytic effect of Ti6Al4V alloy on the diamond. The transition elements can catalyze the phase change of the diamond structure. Moreover, the amorphous C atoms diffuse into the workpiece layer, i.e., diffusion wear. In order to suppress the damaging behavior of the workpiece on the tool, a graphene nanofluid is introduced during the machining process. Figure 3(a1–a5) represent the tool wear process under graphene nanofluid. The tendency of tool wear area reduction is observed. When the model nanofluid is present, the cutting tool changes to a combination of graphene and diamond. The graphene structure is more stable and has high thermal conductivity, thus protecting the diamond tool. The nanofluid impedes the impact and catalytic effect of the Ti6Al4V alloy workpiece on the tool. As a result, the number of amorphous C atoms is reduced by the action of graphene nanofluid, and tool wear is suppressed.

3.3. Thermal Fluctuations during Cutting Simulation

In machining, the contact interface between the tool and the workpiece experiences shear and plastic deformation due to friction, leading to heat generation. Although the chips carry away part of the cutting heat, most are still stored in the workpiece. Especially when machining Ti6Al4V alloy with low thermal conductivity, it is difficult to diffuse the chip heat in time, so the temperature in the cutting area gradually accumulates. Increased temperature will increase tool wear, surface roughness, and changes in workpiece properties. During the utilization of diamond tools, controlling the cutting temperature is a crucial factor in ensuring the service life of the tool. The structure of the diamond is easily disrupted at high temperatures. It causes the way the carbon atoms are bonded to be altered

so that the otherwise very hard diamond material becomes relatively soft. The original hardness and wear resistance are reduced. To investigate the suppression effect of graphene nanofluid on temperature, the thermal effect was analyzed during the molecular dynamics cutting simulation. Figure 4 shows the variation process of cutting temperature of the tool and workpiece with machining distance. The cutting temperature variation processes under dry and graphene nanofluid are represented by red and black curves, respectively. Under dry conditions, the cutting heat of the tool undergoes significant fluctuations. The cutting temperature shows a trend of increasing at the beginning and then decreasing with the increase in cutting distance and a more stable trend at the end. The tool is forced into full contact with the workpiece as the cutting distance increases. The cutting motion of the tool becomes stable. The average cutting temperature at this time is about 600 K. The cutting temperature in the graphene nanofluid environment is smoother relative to the dry cutting. The average cutting temperature gradually rises to equilibrium as the cutting distance increases. At this point, the maximum cutting temperature is 466 K. Both the peak and fluctuation are mitigated compared to dry cutting. Simulation results show that graphene nanofluid effectively suppresses the process of high-temperature transfer from the contact area to the tool. The stability of the diamond structure was ensured. Thus, the graphene nanofluid improved the thermal vibration state of atoms in the diamond structure and suppressed the distortion and breakage of C-C bonds.

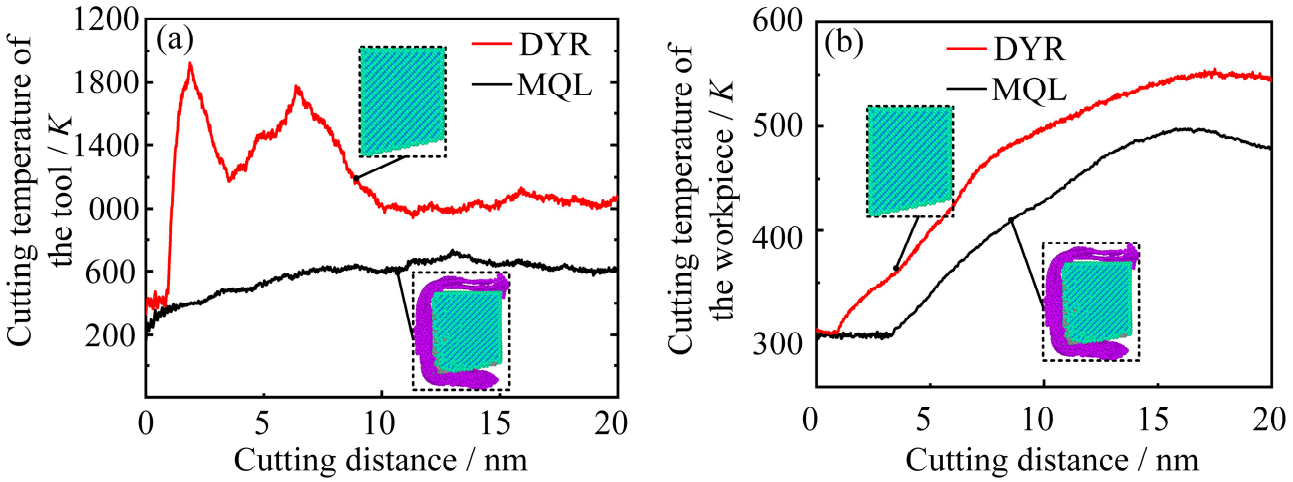

Figure 4. Tool and workpiece temperature profiles during cutting simulation. (**a**) Tool and (**b**) workpiece.

In addition, the average cutting temperature of the workpiece was also analyzed, as shown in Figure 4b. The cutting temperature in both working conditions showed an increasing trend with the increase in cutting distance. However, the cutting temperature under graphene nanofluid lubrication and cooling is much lower. This is mainly because the friction coefficient at the workpiece–tool interface is larger than the workpiece–graphene–tool friction coefficient, and the larger the friction coefficient, the more heat is generated. Excessive heat not only aggravates tool wear but also affects the steady state of the workpiece structure and the quality of the machined surface. Therefore, graphene nanofluid can effectively suppress tool wear and improve machining performance.

3.4. Cutting Force and Cutting Efficiency during Cutting Simulation

The magnitude of cutting force in machining has a great impact on machining accuracy, surface quality, and machining efficiency. The cutting force is influenced by several factors, such as cutting speed, feed, depth of cut, and material hardness. Generally speaking, the relationship between cutting force and speed is relatively complex [10]. In this study, cutting force variations during the cutting simulation were analyzed to investigate the effect of graphene nanofluid on cutting performance. Figure 5 shows the cutting force variation during the cutting simulation under two working conditions, where red represents the dry

cutting simulation, and black represents the graphene nanofluid environment simulation. The cutting force shows an increasing trend with the increased machining distance in the dry condition. It indicates that the reaction force that hinders the tool motion gradually increases. Therefore, the increase in reaction force will further increase the pulling force of the workpiece atoms on the tool atoms, eventually leading to the breakage of the C-C bond. When the C-C bond of the diamond structure is broken, the hardness and wear resistance of the diamond decreases. Tool wear is more likely to occur as the wear increases. Therefore, diamond tool wear exhibits a non-linear increase with increasing machining distance during dry cutting. The cutting force at the same working condition decreases under the effect of graphene nanofluid. The cutting force was reduced from 160 nN to 102 nN. It indicates that graphene changed the contact properties between the tool–workpiece interface. The nanofluid acted as a lubricant between the friction interfaces. It is mainly because the interaction force of the Ti6Al4V workpiece atoms on the C atoms of the graphene structure is lower than that on the C atoms of the diamond structure. Therefore the pulling force of the workpiece on the tool is reduced. The graphene nanofluid relieves the C-C bond breakage of the diamond structure. In addition, the graphene structure is more chemically inert, and it is difficult for Ti6Al4V alloy workpieces to form a catalytic effect on it. Graphene inhibits the diffusion wear of diamond tools. Therefore, the cutting force is lower, and tool wear is suppressed under the graphene nanofluid.

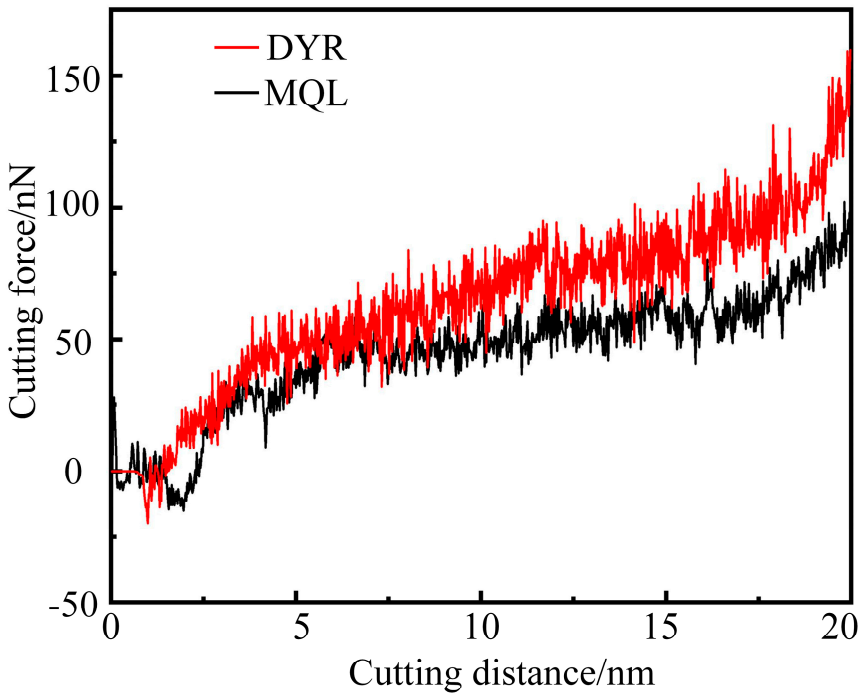

Figure 5. Cutting force variation under dry and MQL conditions. Red and black lines represent cutting forces in dry environment and graphene nanofluid, respectively.

During the cutting process, shear and pressure are generated in the contact area between the tool and the workpiece, resulting in the removal of atoms from the surface of the workpiece. It can be seen from Figure 6a,b that the width of the cut groove under dry cutting conditions is approximately 28 Å. As the cutting distance increases, chips are accumulated on the front face. However, the cutting contour is not the same as the tool profile but has an irregular elliptical shape, as shown in Figure 6c. It is mainly because the chemical bonds between the workpiece atoms are not completely broken during cutting. Elastic recovery occurs after the tool has passed through. When graphene nanofluid was introduced, the cutting width increased to 36 Å. At the same time, we found that the cutting profile became more regular, as shown in Figure 6f. Therefore, the graphene nanofluid improves the material removal efficiency. Although the cutting efficiency per

unit of time increases, the cutting force for the same working condition is less, as shown in Figure 5. The tool wear is lower, as shown in Figure 2. The results show that the graphene nanofluid improves the tool–workpiece contact characteristics, and the tool wear is effectively suppressed.

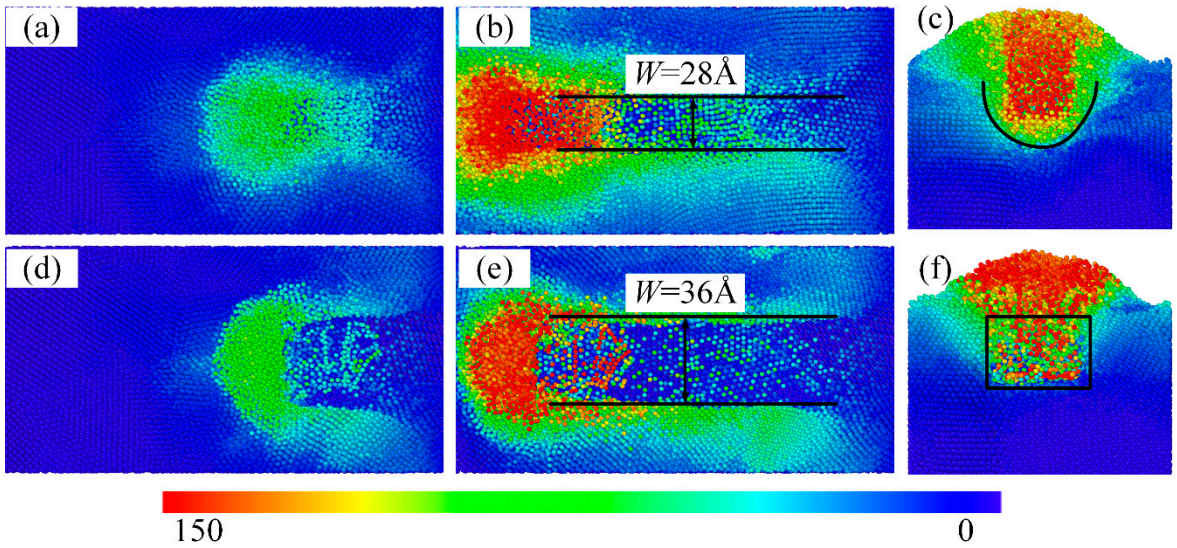

Figure 6. Workpiece surface profile. (**a**–**c**) Graphene nanofluid environment. (**d**–**f**) Dry environment.

4. Conclusions

In summary, MD simulation and the micro-milling experiences are carried out to explore the suppression mechanism of graphene nanofluid for tool wear. Firstly, the profile of tool wear under dry and nanofluid environments is observed by SEM. Next, through molecular dynamics simulation, the suppression mechanism of graphene nanofluid is revealed from the perspective of atomic morphology, cutting temperature, cutting force, and cutting profile. The conclusions can be summarized as follows:

- Although the diamond has a very high hardness, noticeable wear behavior is observed during the micro-milling experiment of the Ti6Al4V alloy. Diamond tools primarily experience adhesive wear and abrasive wear in dry environments. However, tool wear is effectively suppressed under the graphene nanofluid MQL;
- The amorphization behavior of diamond tools is observed during the simulation of cutting titanium alloy. The C-C bonds in diamonds are broken under extreme loads and catalytic effects of the workpiece elements, which is the main cause of tool wear. However, it is observed that the number of amorphous atoms in the graphene nanofluid environment is significantly lower compared to the dry environment. Therefore, the graphene nanofluid suppressed the wear of diamond tools caused by amorphization;
- The tool–workpiece interface properties are modified by graphene nanofluid during micro-milling. The graphene prevents the direct impact of the workpiece on the tool. The adsorption capacity of workpiece atoms to diamond C atoms is reduced. The molecular dynamics simulation results showed that the cutting forces and cutting temperatures are reduced by graphene nanofluid. As a result, the stability of the tool lattice structure is improved;
- Not only is tool wear effectively suppressed by the graphene nanofluid, but the contact area between the tool and the workpiece material is also increased, improving processing efficiency. Moreover, the surface profile of the workpiece was more regular under the graphene nanofluid.

Author Contributions: H.W.: conceptualization, methodology, software, formal analysis, writing-original draft; Q.B.: resources, supervision, project administration, funding acquisition; S.C.: data curation, writing—review & editing; Y.D.: visualization; W.G.: writing—review & editing; T.W.: writing-review & editing. All authors have read and agreed to the published version of the manuscript.

Funding: This research was funded by the National Natural Science Foundation of China (52075129) and NSAF (U2030109).

Data Availability Statement: The data presented in this study are available on request from the corresponding author.

Acknowledgments: The authors would like to deeply appreciate the support from the National Natural Science Foundation of China (52075129) and NSAF (U2030109).

Conflicts of Interest: The authors declare no conflict of interest.

References

1. Niinomi, M. Recent applications, research and development in titanium and its alloys. *Tetsu Hagane-J. Iron Steel Inst. Jpn.* **2004**, *90*, 462–471. [CrossRef] [PubMed]
2. Boyer, R.R. An overview on the use of titanium in the aerospace industry. *Mater. Sci. Eng. A-Struct. Mater. Prop. Microstruct. Process.* **1996**, *213*, 103–114. [CrossRef]
3. Cui, C.; Hu, B.; Zhao, L.; Liu, S. Titanium alloy production technology, market prospects and industry development. *Mater. Des.* **2011**, *32*, 1684–1691. [CrossRef]
4. Liu, S.; Shin, Y.C. Additive manufacturing of Ti6Al4V alloy: A review. *Mater. Des.* **2019**, *164*, 107552. [CrossRef]
5. Gadakh, V.S.; Badheka, V.J.; Mulay, A.S. Solid-state joining of aluminum to titanium: A review. *Proc. Inst. Mech. Eng. Pt. L-J. Mater.-Design Appl.* **2021**, *235*, 1757–1799. [CrossRef]
6. Rafi, H.K.; Karthik, N.V.; Gong, H.; Starr, T.L.; Stucker, B.E. Microstructures and Mechanical Properties of Ti6Al4V Parts Fabricated by Selective Laser Melting and Electron Beam Melting. *J. Mater. Eng. Perform.* **2013**, *22*, 3872–3883. [CrossRef]
7. Zha, J.; Villarrazo, N.; de Pisson, G.M.; Li, Y.; Zhang, H.; de Lacalle, L.N.L. An accuracy evolution method applied to five-axis machining of curved surfaces. *Int. J. Adv. Manuf. Technol.* **2023**, *125*, 3475–3487. [CrossRef]
8. Love, S.; Hertzberg, A.; Woodcock, G. Lunar-derived titanium alloys for hydrogen storage. *J. Propul. Power* **1992**, *8*, 869–872. [CrossRef]
9. Calleja, A.; Alonso, M.A.; Fernandez, A.; Tabernero, I.; Ayesta, I.; Lamikiz, A.; de Lacalle, L.N.L. Flank milling model for tool path programming of turbine blisks and compressors. *Int. J. Prod. Res.* **2015**, *53*, 354–3369. [CrossRef]
10. Duan, Z.; Li, C.; Ding, W.; Zhang, Y.; Yang, M.; Gao, T.; Cao, H.; Xu, X.; Wang, D.; Mao, C.; et al. Milling Force Model for Aviation Aluminum Alloy: Academic Insight and Perspective Analysis. *Chin. J. Mech. Eng.* **2021**, *34*, 18. [CrossRef]
11. Pramanik, A. Problems and solutions in machining of titanium alloys. *Int. J. Adv. Manuf. Technol.* **2014**, *70*, 919–928. [CrossRef]
12. M'Saoubi, R.; Axinte, D.; Soo, S.L.; Nobel, C.; Attia, H.; Kappmeyer, G.; Engin, S.; Sim, W. High performance cutting of advanced aerospace alloys and composite materials. *CIRP Ann.-Manuf. Technol.* **2015**, *64*, 557–580. [CrossRef]
13. Du, Q.; Wang, X.; Zhang, S.; Long, W.; Zhang, L.; Jiu, Y.; Yang, C.; Zhang, Y.; Yang, J. Research status on surface metallization of diamond. *Mater. Res. Express* **2019**, *6*, 122005. [CrossRef]
14. Zhao, Y.; Liu, H.; Yu, T.; Hong, M. Fabrication of high hardness microarray diamond tools by femtosecond laser ablation. *Opt. Laser Technol.* **2021**, *140*, 107014. [CrossRef]
15. Polvorosa, R.; Suarez, A.; de Lacalle, L.N.L.; Cerrillo, I.; Wretland, A.; Veiga, F. Tool wear on nickel alloys with different coolant pressures: Comparison of Alloy 718 and Waspaloy. *J. Manuf. Process.* **2017**, *26*, 44–56. [CrossRef]
16. Suarez, A.; de Lacalle, L.N.L.; Polvorosa, R.; Veiga, F.; Wretland, A. Effects of high-pressure cooling on the wear patterns on turning inserts used on alloy IN718. *Mater. Manuf. Process.* **2017**, *32*, 678–686. [CrossRef]
17. Suarez, A.; Veiga, F.; Polvorosa, R.; Artaza, T.; Holmberg, J.; de Lacalle, L.N.L.; Wretland, A. Surface integrity and fatigue of non-conventional machined Alloy 718. *J. Manuf. Process.* **2019**, *48*, 44–50. [CrossRef]
18. Lee, Y.J.; Hao, L.; Lüder, J.; Chaudhari, A.; Wang, S.; Manzhos, S.; Wang, H. Micromachining of ferrous metal with an ion implanted diamond cutting tool. *Carbon* **2019**, *152*, 598–608. [CrossRef]
19. Huang, S.; Liu, X.; Chen, F.Z.; Zheng, H.X.; Yang, X.L.; Wu, L.B.; Song, J.L.; Xu, W.J. Diamond-cutting ferrous metals assisted by cold plasma and ultrasonic elliptical vibration. *Int. J. Adv. Manuf. Technol.* **2016**, *85*, 673–681. [CrossRef]
20. Du, J.B.; Zhang, Q.; Zong, W.J. Summary of single point diamond turning technology for hard, brittle and ferrous metal materials. *J. Mech. Eng.* **2023**, *59*, 156–175.
21. Zhang, Y.; Zhou, Z.; Wang, J.; Li, X. Diamond Tool Wear in Precision Turning of Titanium Alloy. *Mater. Manuf. Process.* **2013**, *28*, 1061–1064. [CrossRef]
22. Zareena, A.R.; Veldhuis, S.C. Tool wear mechanisms and tool life enhancement in ultra-precision machining of titanium. *J. Mater. Process. Technol.* **2012**, *212*, 560–570. [CrossRef]
23. Park, K.; Beal, A.; Kim, D.D.; Kwon, P.; Lantrip, J. Tool wear in drilling of composite/titanium stacks using carbide and polycrystalline diamond tools. *Wear* **2011**, *271*, 2826–2835. [CrossRef]

24. Gonzalez, H.; Pereira, O.; de Lacalle, L.N.L.; Calleja, A.; Ayesta, I.; Munoa, J. Flank-milling of integral blade rotors made in Ti6Al4V using cryo CO_2 and minimum quantity lubrication. *J. Manuf. Sci. Eng.-Trans. ASME* **2021**, *143*, 091011. [CrossRef]
25. Villarrazo, N.; Caneda, S.; Pereira, O.; Rodriguez, A.; de Lacalle, L.N.L. The effects of lubricooling ecosustainable techniques on tool wear in carbon steel milling. *Materials* **2023**, *16*, 2936. [CrossRef]
26. Pereira, O.; Celaya, A.; Urbikain, G.; Rodriguez, A.; Fernandez-Valdivielso, A.; de Lacalle, L.N.L. CO_2 cryogenic milling of Inconel 718: Cutting forces and tool wear. *J. Mater. Res. Technol-JMRT* **2020**, *9*, 8459–8468. [CrossRef]
27. Amigo, F.J.; Urbikain, G.; Pereira, O.; Fernandez-Lucio, P.; Fernandez-Valdivielso, A.; de Lacalle, L.N.L. Combination of high feed turning with cryogenic cooling on Haynes 263 and Inconel 718 superalloys. *J. Manuf. Process.* **2020**, *58*, 208–222. [CrossRef]
28. Sidik, N.A.C.; Samion, S.; Ghaderian, J.; Yazid, M.N.A.W. Recent progress on the application of nanofluids in minimum quantity lubrication machining: A review. *Int. J. Heat Mass Transf.* **2017**, *108*, 79–89. [CrossRef]
29. Sharma, A.K.; Tiwari, A.K.; Dixit, A.R. Progress of Nanofluid Application in Machining: A Review. *Mater. Manuf. Process.* **2015**, *30*, 813–828. [CrossRef]
30. Piratheepan, M.; Anderson, T.N. An experimental investigation of turbulent forced convection heat transfer by a multi-walled carbon-nanotube nanofluid. *Int. Commun. Heat Mass Transf.* **2014**, *57*, 286–290. [CrossRef]
31. Sharma, A.K.; Singh, R.K.; Dixit, A.R.; Tiwari, A.K. Novel uses of alumina-MoS2 hybrid nanoparticle enriched cutting fluid in hard turning of AISI 304 steel. *J. Manuf. Process.* **2017**, *30*, 467–482. [CrossRef]
32. Gupta, M.K.; Song, Q.; Liu, Z.; Sarikaya, M.; Jamil, M.; Mia, M.; Singla, A.K.; Khan, A.M.; Khanna, N.; Pimenov, D.Y. Environment and economic burden of sustainable cooling/lubrication methods in machining of Inconel-800. *J. Clean. Prod.* **2021**, *287*, 125074. [CrossRef]
33. Barai, D.P.; Bhanvase, B.A.; Sonawane, S.H. A Review on Graphene Derivatives-Based Nanofluids: Investigation on Properties and Heat Transfer Characteristics. *Ind. Eng. Chem. Res.* **2020**, *59*, 10231–10277. [CrossRef]
34. Arshad, A.; Jabbal, M.; Yan, Y.; Reay, D. A review on graphene based nanofluids: Preparation, characterization and applications. *J. Mol. Liq.* **2019**, *279*, 444–484. [CrossRef]
35. Rakesh, P.R.; Chakradhar, D. Investigation on the Effect of Graphene Nano-Cutting Fluid Minimum Quantity Lubrication on the Machining Performance of Inconel 625. *Arab. J. Sci. Eng.* **2022**, *47*, 8469–8483. [CrossRef]
36. Anandan, V.; Naresh Babu, M.; Vetrivel Sezhian, M.; Yildirim, C.V.; Dinesh Babu, M. Influence of graphene nanofluid on various environmental factors during turning of M42 steel. *J. Manuf. Process.* **2021**, *68*, 90–103. [CrossRef]
37. Kursus, M.; Liew, P.J.; Che Sidik, N.A.; Wang, J. Recent progress on the application of nanofluids and hybrid nanofluids in machining: A comprehensive review. *Int. J. Adv. Manuf. Technol.* **2022**, *121*, 1455–1481. [CrossRef]
38. Huang, S.Q.; Wu, H.; Jiang, Z.Y.; Huang, H. Water-based nanosuspensions: Formulation, tribological property, lubrication mechanism, and applications. *J. Manuf. Process.* **2021**, *71*, 625–644. [CrossRef]
39. Singh, R.K.; Sharma, A.K.; Bishwajeet Mandal, V.; Gaurav, K.; Nag, A.; Kumar, A.; Dixit, A.R.; Mandal, A.; Das, A.K. Influence of graphene-based nanofluid with minimum quantity lubrication on surface roughness and cutting temperature in turning operation. *Mater. Today-Proc.* **2018**, *5*, 24578–24586. [CrossRef]
40. Thompson, A.P.; Aktulga, H.M.; Berger, R.; Bolintineanu, D.S.; Brown, W.M.; Crozier, P.S.; In't Veld, P.J.; Kohlmeyer, A.; Moore, S.G.; Nguyen, T.D.; et al. LAMMPS—A flexible simulation tool for particle-based materials modeling at the atomic, meso, and continuum scales. *Comput. Phys. Commun.* **2022**, *271*, 108171. [CrossRef]
41. Fan, P.; Goel, S.; Luo, X.; Yan, Y.; Geng, Y.; Wang, Y. An atomistic investigation on the wear of diamond during atomic force microscope tip-based nanomachining of gallium arsenide. *Comput. Mater. Sci.* **2021**, *187*, 110115. [CrossRef]
42. Fung, K.Y.; Tang, C.Y.; Cheung, C.F. Molecular dynamics analysis of the effect of surface flaws of diamond tools on tool wear in nanometric cutting. *Comput. Mater. Sci.* **2017**, *133*, 60–70. [CrossRef]
43. Xu, S.; Wan, Q.; Sha, Z.; Liu, Z. Molecular dynamics simulations of nano-indentation and wear of the γTi-Al alloy. *Comput. Mater. Sci.* **2015**, *110*, 247–253. [CrossRef]
44. Dong, G.; Wang, X.; Gao, S. Molecular dynamics simulation and experiment research of cutting-tool wear mechanism for cutting aluminum alloy. *Int. J. Adv. Manuf. Technol.* **2018**, *96*, 1123–1137. [CrossRef]
45. Zhao, P.; Wu, J.; Chen, H.; Liu, H.; Li, D.; Tan, J. Molecular dynamics simulation study of interaction mechanism between grain boundaries and subgrain boundaries in nano-cutting. *J. Manuf. Process.* **2021**, *67*, 418–426. [CrossRef]
46. Stukowski, A. Visualization and analysis of atomistic simulation data with OVITO—The Open Visualization Tool. *Model. Simul. Mater. Sci. Eng.* **2010**, *18*, 15012. [CrossRef]
47. Mendelev, M.I.; Underwood, T.L.; Ackland, G.J. Development of an interatomic potential for the simulation of defects, plasticity, and phase transformations in titanium. *J. Chem. Phys.* **2016**, *145*, 154102. [CrossRef]
48. Ghiringhelli, L.M.; Valeriani, C.; Los, J.H.; Meijer, E.J.; Fasolino, A.; Frenkel, D. State-of-the-art models for the phase diagram of carbon and diamond nucleation. *Mol. Phys.* **2008**, *106*, 2011–2038. [CrossRef]
49. Zhao, H.; Min, K.; Aluru, N.R. Size and Chirality Dependent Elastic Properties of Graphene Nanoribbons under Uniaxial Tension. *Nano Lett.* **2009**, *9*, 3012–3015. [CrossRef]
50. Goel, S.; Luo, X.; Agrawal, A.; Reuben, R.L. Diamond machining of silicon: A review of advances in molecular dynamics simulation. *Int. J. Mach. Tools Manuf.* **2015**, *88*, 131–164. [CrossRef]
51. Ou, P.; Cao, Z.; Rong, J.; Yu, X. Molecular Dynamics Study on the Welding Behavior in Dissimilar TC4-TA17 Titanium Alloys. *Materials* **2022**, *15*, 5606. [CrossRef]

52. Wu, J.; Lin, S.; Yeh, J.; Chen, S.; Huang, Y.; Chen, H. Adhesive wear behavior of AlxCoCrCuFeNi high-entropy alloys as a function of aluminum content. *Wear* **2006**, *261*, 513–519. [CrossRef]
53. Kim, S.; Le, D.; Lee, S.; Song, K.; Lee, D. Experiment-based statistical prediction on diamond tool wear in micro grooving NiP alloys. *Diam. Relat. Mat.* **2014**, *41*, 6–13. [CrossRef]
54. Chon, K.S.; Takahashi, H.; Namba, Y. Wear inspection of a single-crystal diamond tool used in electroless nickel turning. *Opt. Eng.* **2014**, *53*, 34102. [CrossRef]